Journal of Materials Processing Tech. 256 (2018) 183–189

Contents lists available at ScienceDirect

Journal of Materials Processing Tech.

journal homepage: www.elsevier.com/locate/jmatprotec

Ultrasonic additive manufacturing of steel: Method, post-processing treatments and properties

Asaf Levy[a], Aslan Miriyev[b,*], Niyanth Sridharan[c], Tianyang Han[d], Eran Tuval[a], Sudarsanam Suresh Babu[c], Marcelo J. Dapino[d], Nachum Frage[a]

[a] Department of Materials Engineering, Ben-Gurion University of the Negev, P.O. Box 653, Beer-Sheva, 8410501, Israel
[b] Department of Mechanical Engineering, Columbia University in the City of New York, 500W. 120th St., Mudd 220, New York, NY, 10027, USA
[c] Department of Mechanical, Aerospace and Biomedical Engineering, University of Tennessee, Knoxville, TN, 37996, USA
[d] Department of Mechanical and Aerospace Engineering, The Ohio State University, Columbus, OH, 43210, USA

ARTICLE INFO

Keywords:
Ultrasonic additive manufacturing
Low-alloy carbon steel
Interface
Post-treatment
Spark plasma sintering
Hot isostatic press

ABSTRACT

Ultrasonic additive manufacturing (UAM) was applied to fabricate laminated carbon steel structures. The feasibility of UAM to manufacture low-alloy carbon steel samples was proven. Interface investigation of the UAM parts was conducted by SEM, EBSD and TEM analysis. Multiple defects at the interfaces of the as-printed parts were observed. In order to improve the structural homogeneity and mechanical properties of the parts, spark plasma sintering (SPS) and hot isostatic pressing (HIP) post-treatments were applied. As a result, after both treatments, interface defects were healed and the shear strength of the welding interfaces was significantly improved. Treatment by SPS apparatus showed higher shear strength improvements as compared to the HIP-treated specimens.

1. Introduction

Flexibility in fabrication of parts with complex geometries and ability to reduce weight by selective application of materials, along with the capability of related cost reduction, make additive manufacturing (hereafter: “AM”) an attractive processing route for a wide variety of materials. AM approach was successfully applied to a wide range of metals, such as Al, Cu, Ni, Co, Fe, Ti, Ta, W and their alloys (Inconel 625/718, Ti-6Al-4V, Co-26Cr-6Mo-0.2C, 17-4 PH stainless steel, AlSi10 Mg etc.), as reported by Murr et al. (2012) and Vayre (2012).

Because of the steel’s commercial availability, relatively low cost and demanded properties, it is of the industry’s great interest to apply AM on the steel. Numerous research works have been conducted on AM of steel. The main AM techniques used for steel are electron beam melting, selective laser melting, direct energy deposition and laser deposition. The common physics behind these AM methods is to fabricate parts by local melting and rapid solidification of powdered material. The printed parts are subject to complex thermal cycles, which result in dimensional and microstructural changes and undesired residual stresses in parts. Moreover, large number of defects, namely gas porosity and lack of fusion, are frequently formed during this type of fabrication process (Herzog et al., 2016). The above processing technologies have been used for wide variety of steels including stainless steels 304 and 316L (Yu et al., 2013), 304L (Abd-Elghany and Bourell, 2012), 308LSi (Abioye et al.,2016), 316 (Griffith et al., 1996), H13 tool steel (Pinkerton and Li, 2005) and high-silicon steel (Garibaldi et al., 2016). Recently, Hofmann et al. (2014) reported successful AM of graded 304 steel/invar 36 structure. Rombouts et al. (2006) explored the effect of oxygen, carbon, silicon, titanium and copper on the quality of iron based printed objects. Evidently, main defects of the printed parts are associated with melting and solidification.

Solid state processing techniques, such as ultrasonic additive manufacturing (UAM), might avoid these defects. In UAM, 3D structures are created by joining thin metal layers (as thin as 127 μm) on top of each other by applying ultrasonic vibrations along with compressive normal force. The heart of the UAM system contains two transducers, which convert electrical power into high frequency (20 kHz) vibrations, and a sonotrode horn. Commonly controlled parameters in UAM are the ultrasonic amplitude (~ 5–50 μm), the applied normal force (~500-9000 N) and the sonotrode horn travel speed (up to 105 mm s^{-1}), as reported by Dehoff and Babu (2010). Dimensions of the fabricated parts may vary from small to very large (as large as 1.8 × 1.8 × 0.9 m). The UAM process works at temperatures much lower than the melting temperature of raw materials and enables to weld dissimilar materials (Wolcott et al., 2016), embed electronics, sensors and ceramic reinforcements,

* Corresponding author.
E-mail address: aslan.miriyev@columbia.edu (A. Miriyev).

https://doi.org/10.1016/j.jmatprotec.2018.02.001
Received 15 October 2017; Received in revised form 29 January 2018; Accepted 2 February 2018
Available online 05 February 2018
0924-0136/

fiber optics (Friel and Harris, 2013), shape memory alloys (Hahnlen and Dapino, 2014) and thermocouples (Hahnlen and Dapino, 2011), and silicon carbide fibers (Li and Soar, 2008).

Many studies have been conducted in order to gain deep understanding of the UAM process. Most of the studies focus on aluminum and include process parameters optimization (Wolcott et al. 2014), characterization of microstructure (Dehoff and Babu, 2010), study of weld mechanisms (Shimizu et al., 2014) and mechanical properties (Sridharan et al., 2016a). Moreover, characterization and improvement of UAM of multi-material systems, such as Al/Cu (Truog, 2012) and Al/Ti (Wolcott et al., 2016), was reported. Recently, Sridharan et al. (2016b) applied UAM to fabricate SAE1010 steel/Ta bilayer. However, there are no published literature regarding UAM of laminated low-alloy based steel structures with body centered cubic (BCC) crystal structure. Preliminary investigations of UAM of 316L stainless steel by Tuttle (2007) and Gonzalez and Stucker (2012) have shown bonding between the steel foil and baseplate, while the bond quality was limited by the low power (1 kW) and heat input. Since the bond quality of other material systems has been improved with the increase of weld power from 1 kW to 9 kW in recent developments, it is of a great interest to investigate the capability of 9 kW UAM to achieve steel to steel joining and characterize the mechanical and microstructural properties of UAM steel samples. This need forms the motivation behind this research.

Mechanical properties of the UAM-fabricated parts mainly depend on the characteristics of the interface region between the layers, thus achieving continuous and strong interfacial bonding is necessary. Bond formation between metal foils is attributed to plastic deformation, collapsing of asperities, dispersion of oxides and metal to metal contact under pressure. Currently, the UAM process does not always result in robust and repeatable joining of metallic foils. Therefore, post-processing treatments are required to improve the mechanical properties of the UAM parts. Recently, Wolcott et al. (2016) reported significant improvement in shear strength of the UAM Al/Ti parts, achieved by applying uniaxial pressure within spark plasma sintering (SPS) apparatus. Miriyev et al. (2016) studied the Al/Ti interface after SPS treatment and showed that the shear strength of the interface layer was higher than that of the weaker joined material (aluminum). Since bonding between metals with FCC and hexagonal close packed (HCP) structure was successfully improved, the present work focuses on joints between BCC crystal structures.

In the current study, the results of UAM of low-alloy carbon steel (matrix with BCC structure), namely SAE4130, are presented. The printed steel parts were subject to post-processing treatments using SPS apparatus and hot isostatic pressing (HIP). The microstructure and shear strength of the untreated UAM SAE4130, SPS- and HIP-treated parts were investigated.

2. Experimental

The laminated 4130 steel/steel parts (Fig. 1a) were fabricated using Fabrisonic “SonicLayer4000” 9 kW UAM machine (Fabrisonic LLC.) in the Ultrasonic Additive Manufacturing Center at the Ohio State University. The additive ultrasonic welding and subtractive CNC stages are integrated in the system and fully automated to create the samples. Nine annealed 0.127 mm thick and 25.4 mm wide SAE4130 steel foils were welded on to a 12.7 mm thick steel substrate (Fig. 1b). The substrate was machined from a hot-rolled ASTM A36 steel stock. To perform ultrasonic additive manufacturing of the steel/steel structures, screening tests were performed to find the viable weld parameters for steel-steel welding. The process parameters, including vibration amplitude (5–50 μm), weld force (~500-9000 N), weld speed (up to 50 mm s^{-1}) and baseplate temperature (up to 204 °C), were varied during the experiments. It is well established that it is more difficult to achieve desired bonding between the foil and the baseplate, than the bonding between foils. Therefore, successful parameters to achieve foil to baseplate welding can be extended to joining of foil to foil. The SAE4130 steel foil was first deposited on the baseplate and subjected to manual peeling test to estimate the weld quality. Only those weld trials in which the steel foils could not be peeled off were considered successful.

Heat treatments were performed in the SPS apparatus HP D5/1 (FCT System, Rauenstein, Germany) and hot isostatic press (HIP) apparatus (American Isostatic Press, AIP, USA). The process in SPS apparatus was carried out at 950 °C for 30 min holding time under argon atmosphere (10-2 torr) and uniaxial pressure of 25 MPa. Pulse-mode DC current (pulse 5 ms, pause 2 ms) was applied. Cooling rate in SPS apparatus was 0.85 °C/sec (Fig. 1c). The HIP process was carried out at 950 °C for 30 min holding time under isostatic 100 MPa argon pressure. Cooling rate in HIP apparatus was 0.25 °C/sec. Characterization of the microstructure was conducted by optical microscopy (Zeiss, Aalen, Germany), High Resolution Scanning Electron Microscope (HRSEM JEOL JSM-7400F, Japan) and High Resolution Transmission Electron Microscope (HRTEM JEOL JEM-2010F, Japan). Electron backscatter diffraction (EBSD) analysis was performed using the JEOL 6500F SEM FEG microscope with 25 kV acceleration voltage and 4 nA probe current. EBSD samples were sectioned using a low speed saw to prevent microstructural changes. Samples were mounted and polished using standard metallographic techniques.

Shear strength was tested before and after the heat treatments using specially designed tooling (Supplementary Fig. 1). Four samples with 5 × 5 mm dimensions were tested for each treatment condition. Cross-section area of the samples was precisely measured. The shear test specimens were mounted between specially-designed test modules in a way that ensures that shear happened inside the layered structure. The specimen within the test modules was mounted in 50 kN LRX Plus mechanical testing apparatus (Lloyd Instruments, Fareham Hants, UK). Micro hardness test was conducted by using Vickers indenter under 2 Kgf load.

3. Results and discussion

After the screening tests, one set of process parameters, listed in Table 1, was selected for building all samples in this study. Based on the results of the screening tests, possible effect of the baseplate temperature on the microstructure and properties of the UAM-fabricated steels should be further studied. UAM allowed to consistently produce steel to steel bonding at the coupon level. However, some challenges and limits have to be addressed to build high performance UAM laminated steel structures. First, cracks are found along the interface between the steel baseplate and the first layer of the steel foil if the number of layers is larger than 15. Stress concentrations associated with the applied process parameters are, probably, the reason of cracking. Of note that cracking is a key issue that needs to be addressed. Second, SAE4130 steel foils tend to stick to the maraging tool steel-made (grade 18Ni (350)) sonotrode. Nuggets have been accumulated on the surface of the sonotrode after prolonged (more than 15 h) steel foils welding (Fig. 2) and affected the bond quality of the subsequent welds. Thus, modifications to the sonotrode material and coating solutions for the existing one should be further investigated.

Cross-section microstructure examinations of the fabricated UAM parts show that the interfaces between the steel layers are discontinuous and contain a large number of defects (Fig. 3a and b). The defects which are formed during the UAM process mainly depend on the presence of oxides on foils’ surface and roughness of top side of (n-1)th foil. The oxide layer and varied roughness may prevent continuous bonding between the bottom surface of the nth layer and top surface of (n-1)th layer. In addition, high normal force, which is applied by the sonotrode horn (6000 N), plastically deform the steel foils. When one succeeding layer is added, cavities are most likely to form where the steel plastic deformation flow is not sufficient. It has to be mentioned that excessive deformation may also result in breaking of already formed bonds, as reported by Sridharan et al. (2016a, b).

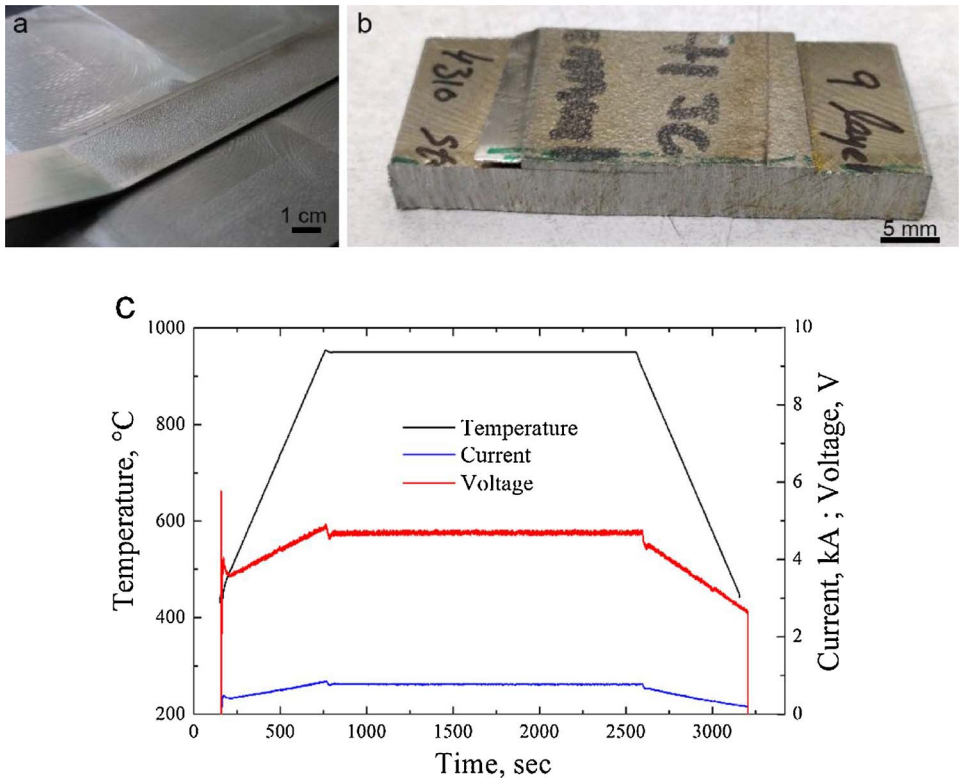

Fig. 1. Steel/Steel laminated part (9 layers on top of the base plate) fabricated using UAM technique (a) and sample prepared for the SPS post-treatment (b); (c) SPS post-treatment parameters (950 °C, 30 min.). Bar size is 1 cm in (a) and 5 mm in (b).

Table 1
UAM process parameters for SAE4130 steel.

	Weld Force	Weld Speed	Amplitude	Nominal Temp.	Horn Texture (Ra)
Level	6000 N	0.021 m/s	30.87 μm	204 °C (400 °F)	14 μm

SPS-treated specimens display only relatively small discontinuity region and small round-shaped voids at the interfaces (Fig. 3c and d). A relatively larger number of discontinuity regions were detected at the sample interfaces after HIP treatment (Fig. 4).

Interestingly, continuous ferrite layer was observed at the interfaces after both post-processing treatments, which was better distinguished by optical microscopy of the etched samples (Fig. 5). The formation of this ferrite layer is a result of the presence of small defects (mostly porous and nonmetallic inclusions) that provide preferential sites for ferrite grains nucleation from austenite, as described below. At elevated temperature (~900 °C) the steel transforms into homogeneous austenite grains. Large voids and defects, presented along the interface, start to "heal", like diffusion bonding mechanisms. In the next step, during cooling from austenite field, the ferrite grains may nucleate at preferential sites, i.e. surrounding the relatively small "healed" voids at the interface. This nucleated ferrite is expected to grow preferentially along the bonded interface and ultimately lead to the observed ferrite-ferrite microstructure. This hypothesis was further investigated using EBSD analysis.

Pearlite is observed only in the interior region of the foils while no pearlite structure is detected at the interface (Fig. 6). The EBSD pattern quality at the interface also shows significant deterioration, which may be attributed to a significant plastic deformation and high dislocation content at the interface (Fig. 6b and c). EBSD image detects a non-symmetric grains refinement across the interface (Fig. 6a). During the UAM process, the sonotrode horn is only in contact with the upper side of the deposited layer and in order to alter the grain size at the bottom side of the foil, a good contact with adjacent layer must be established. However, only partial refinement at the bottom side of the foils was observed in EBSD analysis. It means that during the process the foils were in temporary contact, which was not sufficient to establish adequate bonds and resulted in an interface with large number of defects.

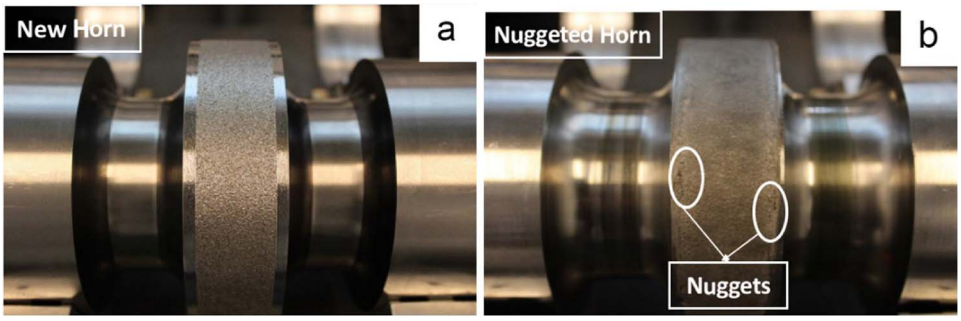

Fig. 2. Newly retextured sonotrode (a) and a sonotrode after approximately 15 h of welding (b).

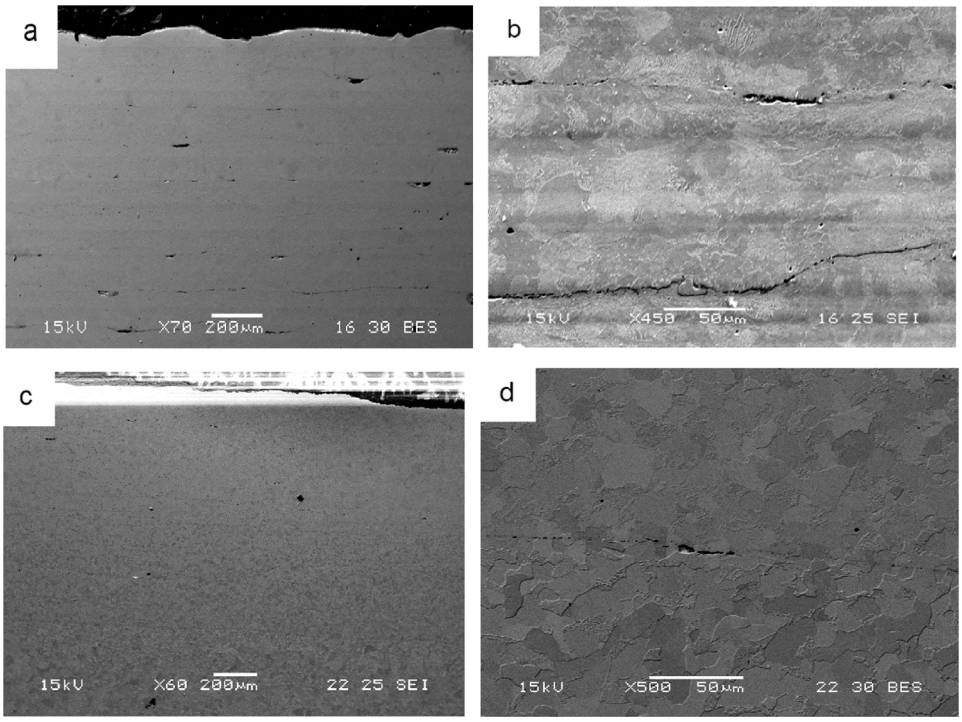

Fig. 3. Macro- and micro-scale scanning electron microscope (SEM) images (secondary electron/backscattered electron) of the specimens' cross-section before (a,b) and after (c,d) the SPS treatment.

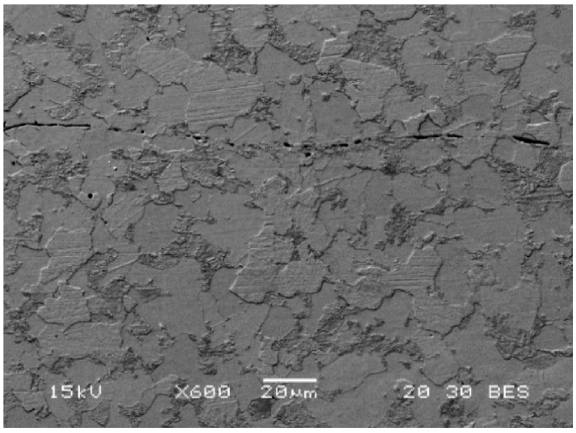

Fig. 4. SEM image of the specimen's cross-section after HIP treatment.

The discontinuities at the interface were, probably, caused by excessive deformation resulting in breaking of the formed bonds.

In the post-treated parts, continuous laminated cross-section was obtained and interfaces between the foils could not be distinguished by the EBSD analysis. Fig. 6d shows the interface region of the as-printed parts compared to that of the HIP-treated ones (Fig. 6e). Similar results were obtained for the samples after the SPS treatment. During both post-treatments, an intimate contact was established between the foils and grain growth took place at the interfaces.

TEM analysis confirmed the presence of BCC ferrite phase with a lattice parameter of 0.292 nm at the interface- value, which is in a good agreement with that reported by Howell and Honeycombe (1982) (Fig. 7a). In addition, grain distribution from very fine grains at the interface to larger grains in the bulk was observed (Fig. 7b). Additionally, TEM analysis indicated the presence of nano-scale inclusions of alumina near the interface (Fig. 7c). These inclusions are typical for steels, already formed during steels fabrication and, generally, homogeneously distributed in steels volume. These inclusions flow, probably,

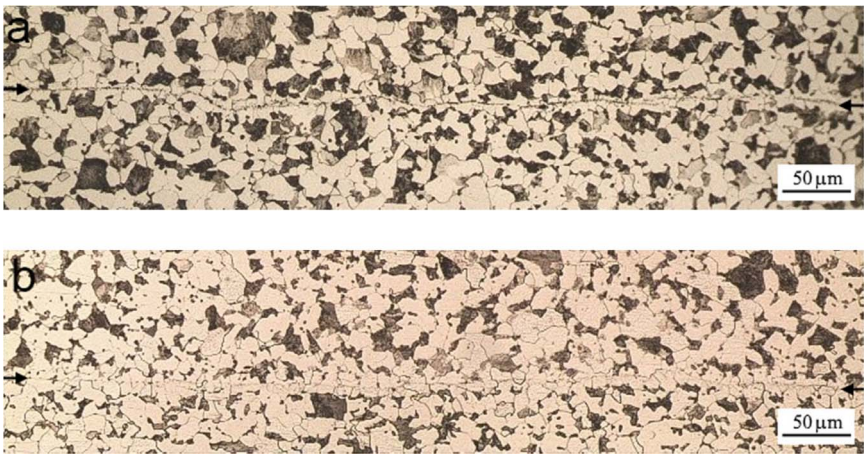

Fig. 5. Optical microscope images (x200) of the SPS-treated (a) and HIP-treated samples (b) after etching. Interfaces between the layers are marked with black arrows at the edges.

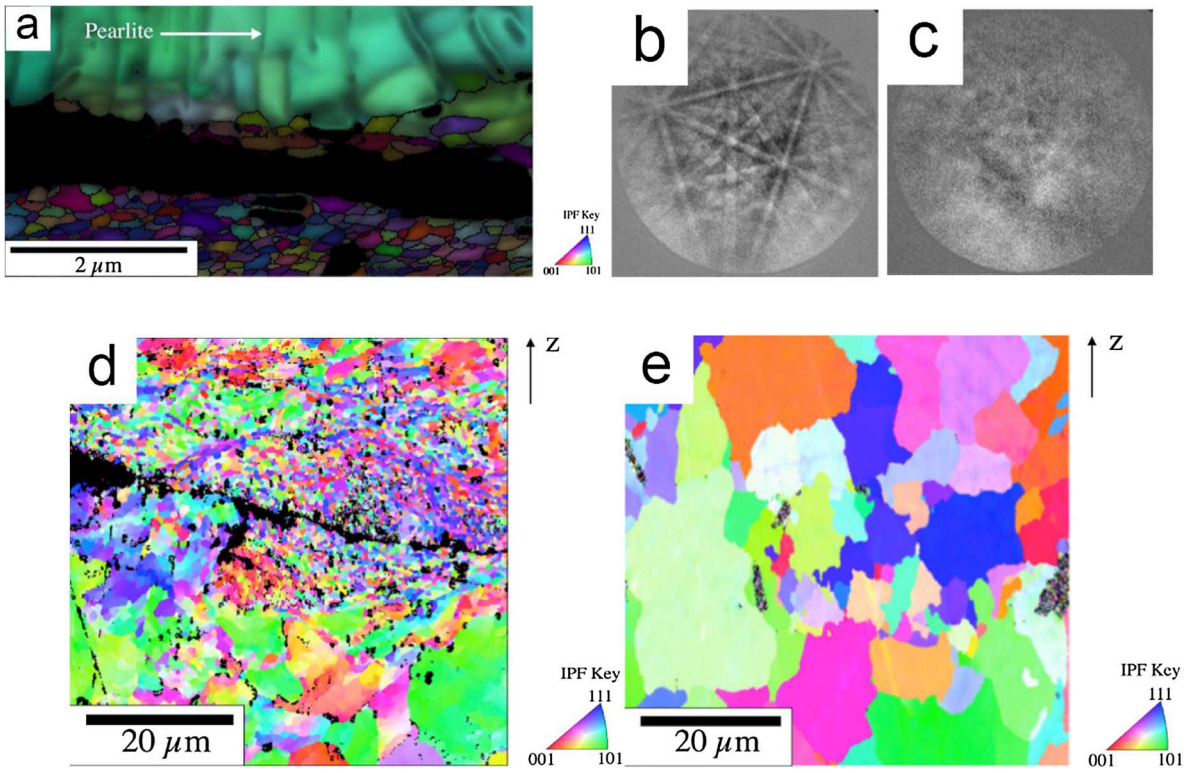

Fig. 6. EBSD images of as-printed and post-treated specimens. (a) High magnification EBSD micrograph and EBSD patterns of the as-printed interface: pattern corresponding to the bulk area (b) and interface area (c); EBSD images of the interface region of the as-printed sample (d) and HIP-treated sample (e).

to the interface due to the plastic deformation of the steel during the UAM process (Fig. 7d).

In order to assess the mechanical properties of the UAM parts and the effect of the post-treatments, shear testing was conducted (Fig. 8). Specimens after the SPS post-treatment exhibit shear strength of about twofold higher than that of the as-printed ones (Fig. 8a and Table 2). Similar observation was obtained by Wolcott et al. (2016) for SPS post-treatment of Al/Ti system fabricated using UAM.

As-printed specimens delaminated and some layers were bent during the shear test. This may be caused by surface roughness of the layers or as a consequence of their small thickness (Fig. 8b). SPS- and HIP-treated samples showed significantly higher resistance to shear. This observation is in a good agreement with the microstructure features obtained after both treatments (Figs. 3 and 4). SPS-treated samples remained mostly intact with some partial deformations (Fig. 8c), while the HIP-treated samples formed “Z-shaped” step (Fig. 8d). Fracture surfaces should be further investigated to gain understanding of the failure mechanisms.

The average micro-hardness of the as-printed samples was measured at 206 ± 20 HV. The hardness values of the SPS-treated samples varied significantly (from 159 to 443 HV) along the Z direction (height). The layers which are close to the base plate exhibit lower hardness values (Table 3). This phenomenon is attributed to the SPS process, in which the top layer is in contact with a graphite punch and some carburization may take place (see the resulted microstructure in the Supplementary Fig. 2). This phenomenon does not occur during the HIP treatment. The average micro-hardness of the HIP-treated samples (153 ± 9 HV) did not depend on layer location. These results are in a good agreement with data reported by Bramfitt (1997) for annealed SAE4130 steel.

4. Conclusions

Laminated low-alloy carbon steel parts were successfully fabricated for the first time using ultrasonic additive manufacturing, opening the door to solid-state layer-by-layer fabrication of steel structures. As-printed parts exhibited numerous defects at the interface affecting the bond quality. SPS- and HIP-post-treatments allowed to significantly decrease the number and size of the defects and to improve the properties of the UAM parts. Shear strength of the SPS-treated samples was almost twofold higher than that of the as-printed parts. Hardness of the SPS-treated samples depended on the layer location with lower values close to the base plate due to intimate contact of the top layer with graphite die, resulting in steel carburization. Average hardness of the HIP-treated samples was about 153 ± 9 HV and did not depend on the layer location. Small ferrite grains are presented along the interface of the post-treated specimens, while inner parts of the layers are mainly comprised larger pearlite grains. The formation of this ferrite layer is a result of the presence of small defects, mostly porous and nonmetallic inclusions, which provide preferential sites for ferrite grains nucleation. TEM analysis indicated the presence of nano-scale inclusions of alumina near the interface. Finally, it was established that laminated carbon steel parts may be fabricated using UAM approach and both SPS- and HIP treatments are suitable for improvement of the mechanical properties of the UAM-fabricated steel parts.

Acknowledgements

Support for T. Han has been provided by the Government of Israel, Ministry of Defense PO No. 444080151. S. S. Babu and N. Sridharan are thankful to the University of Tennessee Knoxville and Oak Ridge National Laboratories/UT-Battelle, LLC. for supporting the microscopy characterization work: This manuscript has been authored by UT-Battelle, LLC, under Contract No. DE-AC05- 00OR22725 with the U.S. Department of Energy. The United States Government retains and the publisher, by accepting the article for publication, acknowledges that the United States Government retains a non-exclusive, paid-up, irrevocable, worldwide license to publish or reproduce the published form of this manuscript, or allow others to do so, for United States Government purposes. The Department of Energy will provide public access to these results of federally sponsored research in accordance

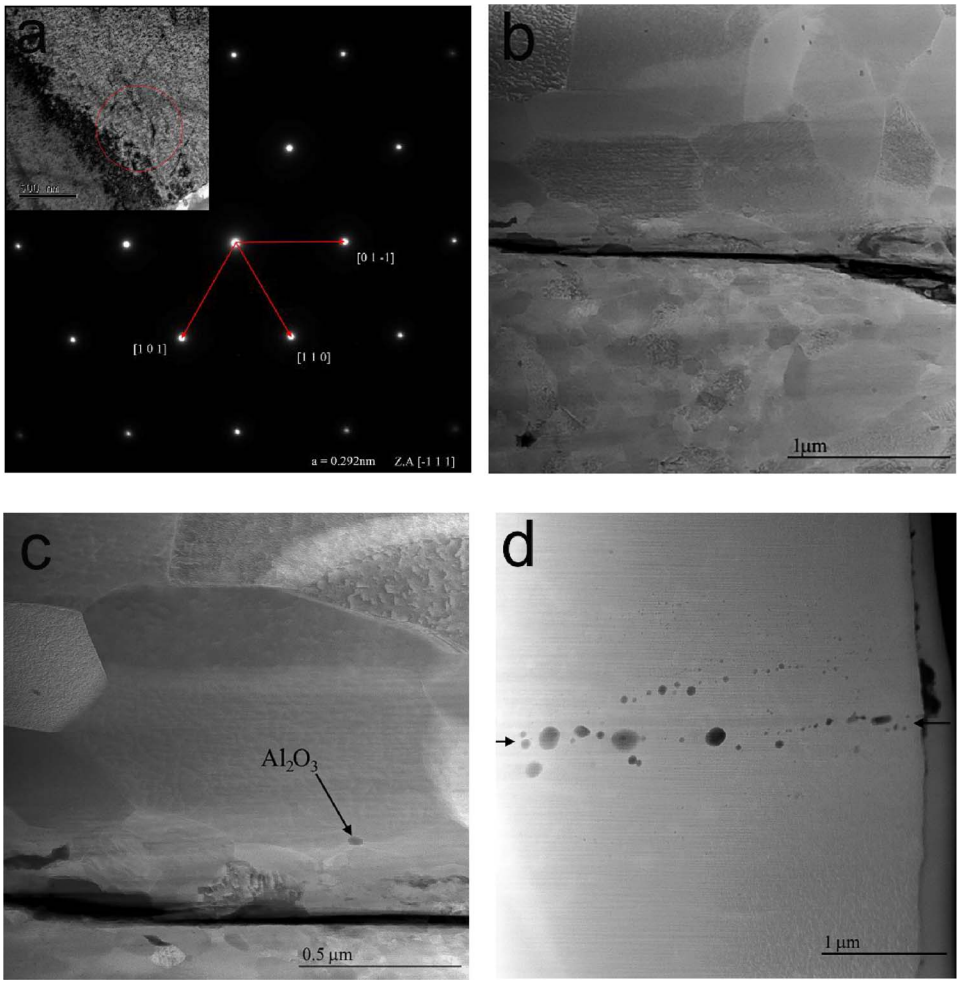

Fig. 7. TEM images of samples' interface. (a) General overview of as-printed interface; (b) magnified image showing alumina particle near the interface; (c) alumina particles close to the joint region (the latter is marked with arrows at the edges); (d) electron diffraction from ferrite grains region near the interface (zone axis [$\bar{1}11$]).

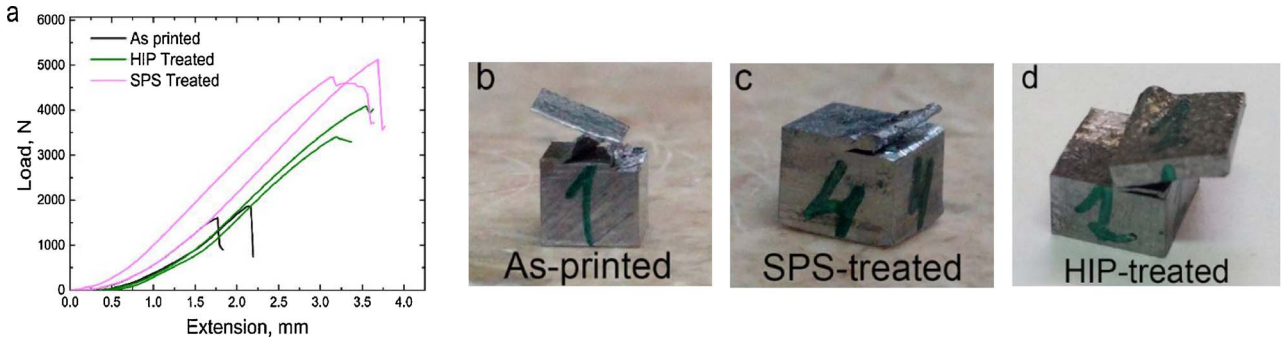

Fig. 8. Shear test. (a) Typical load/displacement curves of the shear test specimens. Two curves are shown for each condition; (b–d) shear test specimens after the test: as-printed specimen (b), SPS-treated specimen (c), HIP-treated specimen (d).

Table 2
Average maximal shear load for as-printed and post-treated specimens.

Sample condition	Average maximal load, N	Standard deviation, N
As-printed	1690	154
SPS-treated	4921	277
HIP-treated	3727	200

Table 3
Hardness values of the UAM laminate after the SPS treatment.

Distance from the lowest layer, μm	Hardness, HV
0	158.6
15	184.7
30	210.2
45	231
60	361.4
70	430.6
90	442.9

with the DOE Public Access Plan (http://energy.gov/downloads/doe-public-access-plan).

Appendix A. Supplementary data

Supplementary material related to this article can be found, in the online version, at doi:https://doi.org/10.1016/j.jmatprotec.2018.02.001.

References

Abd-Elghany, K., Bourell, D.L., 2012. Property evaluation of 304L stainless steel fabricated by selective laser melting. Rapid Prototyp. J. 18, 420–428.

Abioye, T.E., Medrano-Tellez, A., Farayibi, P.K., Oke, P.K., 2016. An investigation into mechanical properties of laser fabricated 308Lsi stainless steel walls by wire feedstock. 30th Int. Conf. Surf. Mod. Tech.

Bramfitt, B.L., 1997. Effects of composition, processing, and structure on properties of irons and steels, materials selection and design. ASM Handbook 20. ASM International, pp. 357–382.

Dehoff, R.R., Babu, S.S., 2010. Characterization of interfacial microstructures in 3003 aluminum alloy blocks fabricated by ultrasonic additive manufacturing. Acta Mater. 58, 4305–4315.

Friel, R.J., Harris, R.A., 2013. Ultrasonic additive manufacturing A hybrid production process for novel functional products. Procedia CIRP 6, 35–40.

Garibaldi, M., Ashcroft, I., Simonelli, M., Hague, R., 2016. Metallurgy of high-silicon steel parts produced using selective laser melting. Acta Mater. 110, 207–216.

Gonzalez, R., Stucker, B., 2012. Experimental determination of optimum parameters for stainless steel 316L annealed ultrasonic consolidation. Rapid Prototyp. J. 18, 172–183.

Griffith, M.L., Keicher, D.M., Atwood, C.L., Romero, Ja., Smugeresky, J.E., Harwell, L.D., Greene, D.L., 1996. Free form fabrication of metallic components using laser engineered net shaping (LENS). Proc. 7th Solid Free. Fabr. Symp. 125–132.

Hahnlen, R., Dapino, M.J., 2011. Performance and modeling of active metal-matrix composites manufactured by ultrasonic additive manufacturing. Proc. SPIE - Int. Soc. Opt. Eng. 7979, 1–13.

Hahnlen, R., Dapino, M.J., 2014. NiTi-Al interface strength in ultrasonic additive manufacturing composites. Compos. Part B Eng. 59, 101–108.

Herzog, D., Seyda, V., Wycisk, E., Emmelmann, C., 2016. Additive manufacturing of metals. Acta Mater. 117, 371–392. http://dx.doi.org/10.1016/j.actamat.2016.07.019.

Hofmann, D.C., Roberts, S., Otis, R., Kolodziejska, J., Dillon, R.P., Suh, J., Shapiro, A.A., Liu, Z.-K., Borgonia, J.-P., 2014. Developing gradient metal alloys through radial deposition additive manufacturing. Sci. Rep. 4, 5357.

Howell, P.R., Honeycombe, R.W.K., 1982. Solid-solid transformation in inorganic materials. In: Int. Conf. on Solid -Solid Phase Transformations. TMS-AIME. Warrendale, PA. pp. 399–425.

Li, D., Soar, R.C., 2008. Plastic flow and work hardening of Al alloy marices during ultrasonic consolidation fibre embedding process. Mater. Sci. Eng. A. 498, 421–429.

Miriyev, A., Levy, A., Kalabukhov, S., Frage, N., 2016. Interface evolution and shear strength of Al/Ti bi-metals processed by a spark plasma sintering (SPS) apparatus. J. Alloys Compd. 678, 329–336.

Murr, L.E., Gaytan, S.M., Ramirez, D.A., Martinez, E., Hernandez, J., Amato, K.N., Shindo, P.W., Medina, F.R., Wicker, R.B., 2012. Metal fabrication by additive manufacturing using laser and electron beam melting technologies. J. Mater. Sci. Technol. 28, 1–14.

Pinkerton, A.J., Li, L., 2005. Direct additive laser manufacturing using gas- and water-atomised H13 tool steel powders. Int. J. Adv. Manuf. Technol. 25, 471–479.

Rombouts, M., Kruth, J.P., Froyen, L., Mercelis, P., 2006. Fundamentals of selective laser melting of alloyed steel powders. CIRP Ann. – Manuf. Technol. 55, 187–192.

Shimizu, S., Fujii, H.T., Sato, Y.S., Kokawa, H., Sriraman, M.R., Babu, S.S., 2014. Mechanism of weld formation during very-high-power ultrasonic additive manufacturing of Al alloy 6061. Acta Mater. 74, 234–243.

Sridharan, N., Gussev, M., Seibert, R., Parish, C., Norfolk, M., Terrani, K., Suresh, S., 2016a. Rationalization of anisotropic mechanical properties of Al-6061 fabricated using ultrasonic additive manufacturing. Acta Mater. 117, 228–237.

Sridharan, N., Norfolk, M., Babu, S.S., 2016b. Characterization of steel-ta dissimilar metal builds made using very high power ultrasonic additive manufacturing (VHP-UAM). Metall. Mater. Trans. A Phys. Metall. Mater. Sci. 47, 2517–2528.

Truog, A.G., 2012. Bond Improvement of Al/Cu Joints Created by Very High Power Ultrasonic Additive Manufacturing. Ohio State University.

Tuttle, R.B., 2007. Feasibility study of 316L stainless steel for the ultrasonic consolidation process. J. Manuf. Process. 9, 87–93.

Vayre, B., 2012. Metallic additive manufacturing: state-of-the-art review and prospects. Mech. Ind. 13, 89–96. http://dx.doi.org/10.1051/meca/2012003.

Wolcott, P.J., Hehr, A., Dapino, M.J., 2014. Optimal welding parameters for very high power ultrasonic additive manufacturing of smart structures with aluminum 6061. Matrix 9059, 1–14.

Wolcott, P.J., Sridharan, N., Babu, S.S., Miriyev, A., Frage, N., Dapino, M.J., 2016. Characterisation of Al–Ti dissimilar material joints fabricated using ultrasonic additive manufacturing. Sci. Technol. Weld. Join. 21, 114–123.

Yu, J., Rombouts, M., Maes, G., 2013. Cracking behavior and mechanical properties of austenitic stainless steel parts produced by laser metal deposition. Mater. Des. 45, 228–235.